Ocean Engineering 319 (2025) 120125

Contents lists available at ScienceDirect

Ocean Engineering

journal homepage: www.elsevier.com/locate/oceaneng

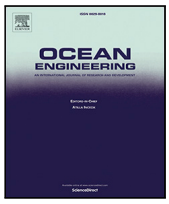

Research paper

Computationally-efficient nonlinear model predictive control of wave energy converters with imperfect wave excitation previews

Siyuan Zhan [a,c], Yutao Chen [b,*], John V. Ringwood [c]

[a] Department of Mechanical, Manufacturing and Biomedical Engineering, Trinity College Dublin, Dublin, D02 PN40, Ireland
[b] School of Electrical Engineering and Automation, Fuzhou University, Fuzhou, 350025, China
[c] Centre for Ocean Energy Research, Maynooth University, Maynooth, W23F2H6, Co. Kildare, Ireland

ARTICLE INFO

Keywords:
Nonlinear model predictive control
Wave prediction
Wave energy converter
Reduced computational complexity

ABSTRACT

Energy maximising (EM) control of wave energy converters (WECs) is a noncausal problem, where wave prediction information can be used to increase the energy conversion rate significantly. However, current approaches do not consider the prediction error evolution in the control formulation process, leading to potential unpredictable performance degradation. Moreover, most existing real-time WEC control approaches assume linear dynamics, motivated by their simplicity and mild computational cost and, thus, are not effective for real-time control for WECs with nonlinear dynamics. Targeting imperfect wave prediction and nonlinear WEC dynamics, this paper proposes a computationally-efficient nonlinear MPC (NMPC) scheme for WECs with (typically) imperfect wave excitation preview. This is achieved by introducing an input move blocking scheme when formulating and solving the online optimisation problem, i.e., defining finer discretisation grids for the control input and wave prediction at the early stages of the prediction horizon, where the wave prediction is more accurate, and coarser grids at the latter stages of the horizon, to reflect less inaccurate wave prediction information. Numerical simulation results are presented, based on a conceptual nonlinear point-absorber WEC, to verify the efficacy of the proposed NMPC method, in terms of produced energy, computational complexity, and robustness against wave prediction inaccuracy.

1. Introduction

Wave energy has significant potential to supply renewable energy to complement other renewable sources. However, the unit cost of current wave energy technology is higher than other renewable (and conventional) sources, and it is well-known that a reliable and efficient wave energy converter (WEC) controller can reduce the unit cost of wave energy (Guo and Ringwood, 2021). However, the effectiveness of early WEC control methods, based on the impedance-matching principle, is challenged to implement when the sea conditions include a wide range of wave frequencies (Zhan and Li, 2019), and when actuator and other safety constraints need to be considered.

The WEC energy maximisation (EM) problem is a non-conventional control problem, where the control objective is to maximise the energy conversion rate, respecting physical system constraints and power take-off torque/force limits. Recent studies reveal that, by fully exploiting excitation force preview, the energy conversion rate can be significantly improved, even trebled in some sea conditions (Babarit and Clément, 2006; Zhan and Li, 2019).

To provide essential non-causal preview information for WEC EM controllers, the wave elevation and wave excitation forecasting problem, within the time scale of several wave periods, has received significant research attention over the past decade. The most popular methods include deterministic sea wave prediction (DSWP) (Belmont et al., 2014), which physically models wave spatial propagation, and time-series approaches, such as autoregressive (AR) models, which exploit the linear statistical nature of the wave at the point of interest (Fusco and Ringwood, 2010; Pena-Sanchez et al., 2018b). While deterministic methods can provide more accurate forecasts for a longer horizon, autoregressive techniques can be more attractive for some applications, since no sensors/instrumentation required (Paparella et al., 2014). An additional complication is that, optimal non-causal controllers require a forecast of the *wave excitation force* (WEF), an unmeasurable quantity, incurring additional estimation errors (Peña-Sanchez et al., 2019), which are further compounded by forecasting errors.

Model predictive control (MPC) provides a natural mechanism to solve the WEC EM control problem. Most real-time MPC WEC controllers assume linear dynamics, motivated by their design simplicity

* Corresponding author.
E-mail address: yutao.chen@fzu.edu.cn (Y. Chen).

https://doi.org/10.1016/j.oceaneng.2024.120125
Received 18 October 2024; Received in revised form 28 November 2024; Accepted 13 December 2024
Available online 30 December 2024

and the low complexity of the associated online optimisation problem. However, this linear assumption may be challenged for some WECs, especially when a WEC is efficiently controlled, due to the amplified device motion under control (Windt et al., 2021), exaggerating nonlinear hydrodynamic effects. The potential sources of those nonlinearities include geometry-induced nonlinearities (Windt et al., 2021), nonlinear Froude–Krylov (FK) static and dynamic forces, nonlinear viscous drag force, and/or nonlinear mooring force (Penalba et al., 2017a). For nonlinear MPC (NMPC), existing approaches, including those based on dynamic programming (Li et al., 2012), Prontragin's minimum principle (Zou et al., 2017), or by directly solving the associated NMPC problem (Tom and Yeung, 2014; Richter et al., 2012; Huang et al., 2024; Demonte Gonzalez et al., 2024), incur severe computational problems and, therefore, are challenging to implement as a real-time WEC controller.

Inspired by the development of the real-time iteration (RTI) framework (Houska et al., 2011), recent studies (Guerrero-Fernández et al., 2022; Haider et al., 2021) have applied the RTI solver to accelerate the computation of NMPC. However, the RTI solver introduced in Houska et al. (2011), originally designed for tracking and regulation problems, require a convex quadratic cost function. Consequently, the WEC NMPC implementations using the RTI framework (Guerrero-Fernández et al., 2022; Haider et al., 2021) must adopt a convex quadratic cost function similar to that used in tracking and regulation problems. This poses a significant challenge, as the energy maximisation objective inherent to WEC NMPC, subject to persistent wave excitations, is inherently non-trivial to represent using such a cost function.

By projecting the input and state onto a set of periodic or pseudo-periodic basis functions, NMPC-like approaches (Faedo et al., 2017) such as pseudo-spectral methods using periodic (Bacelli et al., 2015; Mérigaud and Ringwood, 2017), and non-periodic (Genest and Ringwood, 2016; Li, 2017) basis functions, have been developed for WECs, which show good computational performance. However, a persistent problem is the difficulty in maintaining a convex optimisation problem with nonlinear WEC dynamics. Recently, a moment-matching approach has been used to present a convex formulation for a wide range of nonlinear parameterisations (Faedo et al., 2021), arising from hydrodynamic (Faedo et al., 2022a) or power take-off (PTO) (Faedo et al., 2022b) nonlinearity.

However, in general, these NMPC-like algorithms require high-fidelity wave forecasting in the control formulation, with one notable exception (Faedo et al., 2022c). However, this study (Faedo et al., 2022c) assumes uniform uncertainty in the forecast and cannot exploit information concerning the evolution in uncertainty.

Directly tackling the computational and imperfect prediction issues, this paper develops a real-time implementable, computationally-efficient, NMPC scheme, based on input move blocking (MB). Input MB is a well-known technique, used to reduce the computational complexity in solving the optimisation problem stemming from the MPC formulation. MB reduces the variables to be optimised by enforcing a constant input over several discrete-time steps within the control horizon. In linear MPC, MB is a mature technique with a broad range of applications, including a recent application to WECs (Guerrero-Fernández et al., 2020). However, in NMPC, there are few guidelines for developing MB strategies, especially with the unconventional WEC control objective of maximising energy capture, by exploiting incoming WEF prediction, the accuracy of which deteriorates with the prediction horizon length. In this paper, we propose a novel NMPC framework for the WEC control problem, capable of addressing nonlinear dynamics, unconventional EM control objectives, decreasing wave prediction accuracies, and the computational efficiency requirements of real-time implementation, by introducing an innovative tailored MB structure that enhances computational efficiency while simultaneously mitigating the negative impact of increasing prediction inaccuracies on overall performance. The contributions of this methodology are summarised as follows:

1. A *specific input MB* scheme is designed to suit the WEC NMPC problem, with finer discretisation grids on shorter horizons and coarser grids on longer horizons, which aligns with the relative prediction accuracy. Compared with existing NMPC methods (Guerrero-Fernandez et al., 2023) without input MB, MB-NMPC can achieve better energy conversion efficiency with imperfect predictions, and has significantly less computational complexity, due to the reduced number of decision variables.
2. Targeting the nonlinear programming (NLP) problem stemming from the input MB NMPC, a tailored *condensing strategy* is employed to further reduce the computational complexity, by eliminating state variables from decision variables in the optimisation problem. This is achieved by exploiting the unique structure (denser grid in the near future and coarser grid in the far future) of the optimisation problem stemming from the multiple-shooting-based input MB NMPC applied to a WEC with degraded prediction accuracy. With the tailored condensing strategy, the optimisation problem can be efficiently solved by an active-set method with a 'warm start', i.e. using optimal solutions from the previous sampling instant to initialise the optimisation problem at the current sampling instant.

The remainder of the paper is organised as follows. Section 2 presents the WEC NMPC problem preliminaries, including WEC dynamic modelling and NMPC problem formulation. The main result, i.e. the formulation of the novel input MB NMPC, is presented in Section 3. Implementation issues, including the estimation of full state information, obtaining current and future WEF estimates/predictions, are discussed in Section 4. Demonstrative and comparative examples are given in Section 5, based on a benchmarked WEC described by a nonlinear state-space model. Finally, the paper is concluded in Section 6.

Notation: Let $\mathbb{R}^n$, and $\mathbb{R}^{a\times b}$, denote the space of all real n dimensional vectors, and all a-by-b-dimensional matrices, respectively; $\mathbb{N}_{a:b}$ and $\mathbb{N}_{\geq a}$ denote a set of integers from a to b, and greater than or equal to a, respectively. For column vectors z_1 and z_2, $[z_1, z_2]$ denotes a column vector $[z_1^\top\ z_2^\top]^\top$. $\boldsymbol{z}_{a:b} := [z_a, z_{a+1}, \dots z_b]$. I_n denotes the n-by-n identity matrix. $0_{a\times b}$ denotes an a-by-b matrix composed entirely of zero entries. For $A \in \mathbb{R}^{a\times b}, a > b$, A^+ denotes its (left) pseudo-inverse. "$*$" denotes the convolution operator. "s.t." is the abbreviation of "subject to". "w.r.t." is the abbreviation of "with respect to".

2. Preliminaries

2.1. WEC modelling

Although the proposed method is generic and can be applied to a range of WECs with nonlinear hydrodynamics, in this paper, for demonstration purposes, we present our study on a benchmark point absorber system, restricted to heave motion $z(t)$ only, as shown in Fig. 1.

From Newton's 2nd law, the motion of the float can be described by:

$$M\dot{v}(t) = -f_h(t) - f_{rad}(t) + f_{nl}(t) + f_{ex}(t) + f_u(t), \tag{1}$$

where M is the mass of the free float, while $z(t)$ and $v(t)$ denote heave displacement and heave velocity of the free float w.r.t. the still water level (SWL), respectively. $f_{ex}(t)$ is the wave excitation force, treated as a predictable disturbance input in this paper, while f_u is the manipulated PTO control force. $f_h(t)$ is the hydrostatic restoring force, assumed to be linear for this case, and modelled by:

$$f_h(t) = k_h z(t), \tag{2}$$

with stiffness $k_h = \rho g S_w$, where ρ, g, and S_w denote the water density, gravitational acceleration, and cross-sectional area of the buoy, respectively. $f_{rad}(t)$ models the linear frequency-dependent damping

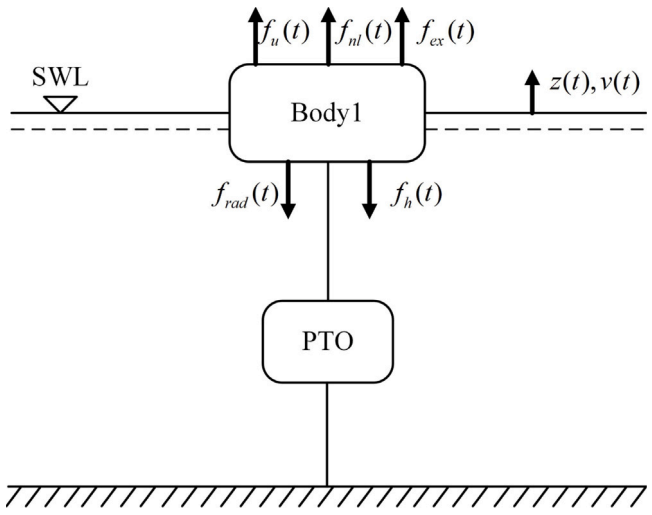

Fig. 1. Dynamic diagram of the float (SWL: still wave level; PTO: power take-off unit).

effect of the radiated waves which, under the standard assumption associated with linear potential theory (Falnes, 2002), is modelled by:

$$f_{rad}(t) = h_r(t) * v(t) + m_\infty \dot{v}(t), \tag{3}$$

where the radiation impulse response $h_r(t)$, and the asymptote of added mass at infinite frequency m_∞, are calculated via a hydrodynamic code such as NEMOH (Penalba et al., 2017b). $f_{nl}(t)$ denotes the total nonlinear effects on the free float. In this paper, we consider a nonlinear viscous drag force for demonstration purposes:

$$f_{nl}(t) = -k_{nl}|v(t)|v(t), \tag{4}$$

where $k_{nl} = \rho C_d A_d$, with drag coefficient C_d and characteristic surface area A_d, which can be determined using methods presented in Giorgi and Ringwood (2017). With (2)–(4), the dynamic equation (1) results in a modified Cummins' (Cummins, 1962) equation:

$$\begin{aligned}(m + m_\infty)\dot{v} = f_{ex}(t) - k_h z(t) - h_r(\tau) * v(t-\tau) \\ - k_{nl}|v(t)|v(t) + f_u(t).\end{aligned} \tag{5}$$

The convolution term in (5) can be approximated with a minimal state-space representation by a number of methods (Peña-Sanchez et al., 2019; Unneland, 2007):

$$\begin{cases} \dot{x}_r(t) = A_r x_r(t) + B_r v(t) \\ y_r(t) = C_r x_r(t) + D_r v(t) \approx h_r(t) * v(t) \end{cases} \tag{6}$$

where $(A_r,\ B_r\ C_r,\ D_r)$, and $x_r \in \mathbb{R}^{n_r}$, are the state-space matrices, and the associated state vector, respectively.

Defining the overall system state vector $x(t) := [z(t),\ v(t),\ x_r(t)]$, where $z(t)$, $v(t)$, $x_r(t)$ are the heave displacement, heave elevation, and the state corresponding to radiation dynamics, respectively, the control input (PTO force) $u(t) := f_u(t)$, and disturbance input (wave excitation force) $w(t) := f_{ex}(t)$, the WEC dynamics described by Cummins' equation (5) can be modelled by the following linear time-variant (LTI) system

$$\begin{aligned}&\dot{x}(t) = Ax(t) + B(w(t) + u(t) - k_{nl}|v(t)|v(t)), \\ &z(t) = C_z x(t), \quad v(t) = C_v x(t),\end{aligned} \tag{7}$$

where

$$A = \begin{bmatrix} 0 & 1 & 0_{1\times n_r} \\ -\frac{k_h}{m} & -\frac{D_r}{m} & -\frac{C_r}{m} \\ 0_{n_r\times 1} & B_r & A_r \end{bmatrix}, \quad B = \begin{bmatrix} 0 \\ \frac{1}{m} \\ 0_{n_r\times 1} \end{bmatrix},$$
$$C_z = \begin{bmatrix} 1 & 0 & 0_{1\times n_r} \end{bmatrix}, \qquad C_v = \begin{bmatrix} 0 & 1 & 0_{1\times n_r} \end{bmatrix}$$

with $m := M + m_\infty$.

2.2. WEC energy maximisation NMPC problem formulation

The WEC control aims to maximise the energy converted in the PTO, $\int p(t)dt$, where $p(t)$ is the instantaneous (electronic) power produced, including the potential electronic losses in the generator (Kody et al., 2019):

$$p(x(t), u(t)) := -v(t)u(t) - ru^2(t). \tag{8}$$

In (8), the first term $-v(t)u(t)$ is converted power (negative heave velocity $v(t)$ multiplied by PTO force $u(t)$, while the second term $-ru^2(t)$ represents electronic energy (copper) losses in generator, with $r > 0$ denoting the coefficient of the quadratic PTO loss. The energy produced, considering energy losses in generator, for a time period from t to $t+T$, can be expressed by:

$$E(t,T) := -\int_t^{t+T} v(\tau)u(\tau) + ru^2(\tau)d\tau. \tag{9}$$

Therefore, minimisation of $-E(t,T)$ in the NMPC problem leads to maximisation of energy produced, considering losses. The WEC is also subject to PTO control force limits:

$$|u(t)| < u_{\max}, \tag{10a}$$

and constraints on heave displacement and heave velocity:

$$|z(t)| \le z_{\max}, \quad |v(t)| \le v_{\max}. \tag{10b}$$

The WEC NMPC problem $\mathcal{P}$ of maximising energy conversion considering electronic losses in the generator (9), while respecting constraints (10), can now be summarised as:

$$\begin{aligned}\mathcal{P}:\ &\min_u \int_t^{t+T} v(\tau)u(\tau) + ru^2(\tau)d\tau, \\ \text{s.t. }\ &\dot{x}(\tau) = Ax(\tau) + B[w(\tau) + u(\tau) - k_{nl}v(\tau)|v(\tau)|], \\ &|z(\tau)| \le z_{\max},\ \ |v(\tau)| \le v_{\max},\ \ |u(\tau)| \le u_{\max}.\end{aligned} \tag{11}$$

Solving NMPC problem $\mathcal{P}$ requires information on the current and future values of WEF $w(t)$, which are non-measurable quantities. Here, we assume imperfect prediction of $w(t)$, from the current time instant t to $t+T$ in the future, which can be obtained from wave prediction techniques, whose prediction accuracy decreases with an increase in horizon. For details on obtaining the WEF preview, please refer to Section 4.

3. Main results - the novel computational approach for the WEC NMPC problem using imperfect wave prediction

The main results of the novel NMPC computational approach are presented in this section. Section 3.1 revisits the NLP formulation using the existing standard uniform grid direct multiple shooting methods. Then, to reduce computational complexity and address imperfect WEF prediction, an input MB reformulation, specifically tailored to the WEC NMPC problem, using a non-uniform parameterisation grid, in line with WEF prediction accuracies, is presented in Section 3.2. In Section 3.3, a *tailored condensing* strategy is developed, exploiting the unique features of the WEC NMPC problem to further accelerate computation. The computational techniques and discontinuity issues of the optimal control input solutions are also discussed in Section 3.3.

3.1. NLP with standard uniform parameterisation grid direct multiple shooting

The continuous-time WEC NMPC problem $\mathcal{P}$, defined in (11), leads to a computationally-intractable infinite dimensional optimisation and, hence, must be discretised into a finite-dimensional problem that can be solved computationally. To address this problem, the standard multiple shooting method (Bock and Plitt, 1984) is adopted to discretise $\mathcal{P}$ into a finite-dimensional NLP problem.

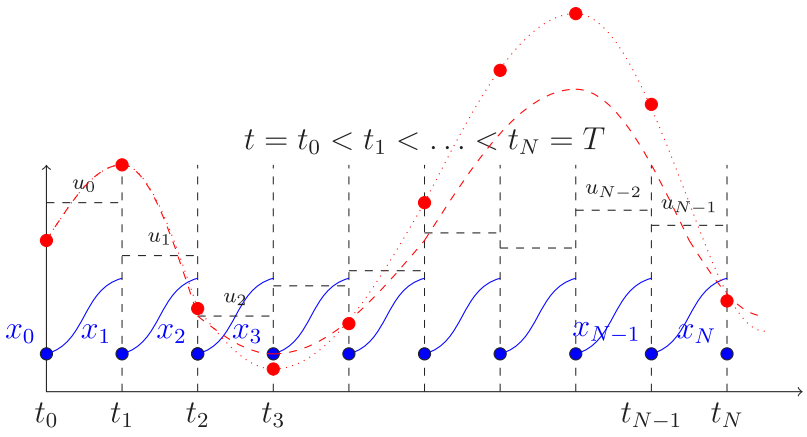

(a) Standard uniform grid parameterisation

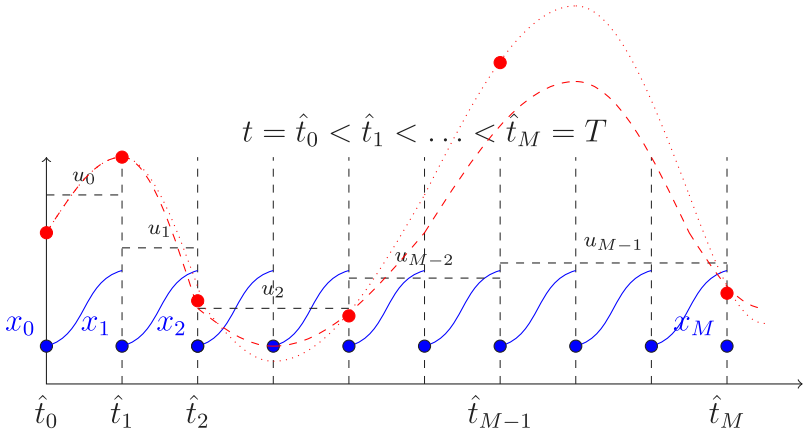

(b) Input block parameterisation with looser grid length at the latter stages of the prediction horizon

Fig. 2. Illustrative diagrams for two different parameterisation strategies: (a) the state, control and wave trajectories are parameterised by N intervals of equal size; (b) the control and wave trajectories are parameterised by M non-equidistant grids, where the grid discretisation becomes looser at the latter stages of the prediction horizon. (solid blue line: x; dashed black line u; dotted red line: the imperfectly predicted WEF $\hat{w}$ used in WEC NMPC; dashed red line: the real WEF w shown as a reference.).

As illustrated in Fig. 2(a), a standard uniform grid is introduced $\boldsymbol{G}_{0:N-1} = [t_0, t_1 \ldots, t_N]$, partitioning the prediction horizon T into N shooting intervals with uniform width. Here, the initial and final values of the grid take the value of the beginning and the ending time instants of the prediction horizon, i.e., $t_0 = t$ and $t_N = t + T$.

Next, the continuous state and wave prediction trajectories x and w are discretised at the $N + 1$ discretisation nodes. The control input is assumed piece-wise constant on each shooting interval. One illustrative example of this standard uniform parametrisation is provided in Fig. 2(a) (x with the solid blue line, u with the dashed black line, and predicted w with the dotted red line, respectively).

With these N equidistant partitions $\boldsymbol{G}_{0:N-1}$, following the standard procedure of direct multiple shooting, the WEC NMPC problem $\mathcal{P}$ is discretised into the following NLP_N, which needs to be solved within one sampling interval, with the explicit subscript N representing the number of partitions:

$$\begin{aligned} \text{NLP}_N: \quad & \min_{\boldsymbol{x}_{0:N}, \boldsymbol{u}_{0:N-1}} \sum_{k=0}^{N-1} h(x_k, u_k, \hat{w}_k) \\ s.t. \quad & x_{k+1} = \phi(x_k, u_k, \hat{w}_k),\ k \in \mathbb{N}_{0:N-1}, \\ & (-z_{\max}, -v_{\max}) \le x_k \le (z_{\max}, v_{\max}),\ k \in \mathbb{N}_{0:N}, \\ & -u_{\max} \le u_k \le u_{\max},\ k \in \mathbb{N}_{0:N-1}. \end{aligned} \tag{12}$$

Here, $h(\cdot,\cdot,\cdot)$ is the objective function that will be calculated in (14); x_k, u_k, $\hat{w}_k$ are the state, the control input, and the predicted WEF, respectively, at time instant t_k, i.e., $x_k := x(t_k)$, $u_k := u(t_k)$, and $\hat{w}_k := \hat{w}(t_k)$, respectively; The symbol $\phi(.,.,.)$ numerically integrates the dynamics in (11), specifically

$$\dot{x}(\tau) = Ax(\tau) + B[w(\tau) + u(\tau) - k_{nl} v(\tau)|v(\tau)|], \tag{13}$$

within one partition, starting from time instant t_k to t_{k+1}, with initial condition $x_k, u_k, \hat{w}_k$, using commonly used integration methods such as Euler or Runge–Kutta. As a result, there are, in total, N integrations within the prediction horizon. Since the control $u(\tau)$ takes a constant value (zero-order hold) within one shooting interval, i.e. $u(\tau) = u_k$ for $t_k \le \tau < t_{k+1}$, the objective function $h(x_k, u_k, \hat{w}_k)$, representing the running cost within one shooting interval, can be described as

$$h(x_k, u_k, \hat{w}_k) = \int_{t_k}^{t_{k+1}} \left[v(\tau)u(\tau) + ru^2(\tau)\right] d\tau = (z_{k+1} - z_k)u_k + R_k u_k^2, \tag{14}$$

where $R_k := r(t_{k+1} - t_k)$, and z_{k+1} is the predicted heave displacement at t_{k+1}, depending on the triple $(x_k, u_k, \hat{w}_k)$.

Upper and lower bound constraints for the state and input variables, at each node in the prediction horizon, are employed.

Note that the dimension of NLP_N is characterised by the number of partitions N, given the fixed state and control space dimensions. On the one hand, a larger N would capture the dynamics (13) more accurately, at the cost of a higher dimensional NLP, which is difficult to solve. On

the other hand, a smaller N would reduce the computational load for solving the NLP, but at the cost of poor dynamics representation. In the specific case of WEC NMPC with imperfect WEF prediction accuracy, it is desired to have an accurate enough capture of WEF dynamics when the prediction is accurate, and, a less exact representation of WEF dynamics when the prediction is relatively inaccurate. This suggests a novel input MB strategy to discretise problem $\mathcal{P}$, as is discussed in Section 3.2.

3.2. Design of a novel input MB strategy considering varying WEF prediction accuracy

Efficient WEC noncausal controllers require a sufficient prediction horizon to achieve desirable performance, at least covering more than one wave period. According to the discussion in Section 3.1, this has two implications: (1) a large number of nodes N is required, leading to increased computational complexity; (2) wave prediction with decreased accuracy over long horizons, when used with a uniform confidence level over the complete prediction horizon, can lead to performance degradation.

To tackle those two issues, an input MB scheme (Chen et al., 2020) is tailored to reflect imperfect (and progressively degrading) $f_{ex}(t)$ prediction. The core idea is to define a non-equidistant shooting interval for the control input and disturbance, denser at earlier points within the control horizon with high prediction confidence and more sparse at later points within the horizon.

Define a new shooting grid $\boldsymbol{G}_{0:M-1}$, with a significantly smaller number of nodes $M \ll N$, but covering the same prediction horizon timespan $\sum_{i=0}^{M-1}(\hat{t}_{i+1}-\hat{t}_i)=\sum_{j=0}^{N-1}(t_{j+1}-t_j)$, and $t_0=\hat{t}_0=t$, $t_N=\hat{t}_M=t+T$. As illustrated in Fig. 2(b), the grid interval length of $\boldsymbol{G}_{0:M-1}$ is a multiple of that of $\boldsymbol{G}_{0:N-1}$, resulting in a total of M interval blocks in the prediction horizon. Define $I=[I_0,\dots,I_M]$ as a vector of the starting index of each block, with N_j, $j\in\mathbb{N}_{0:M-1}$ is the number of shooting intervals contained in the jth block. Since the prediction horizon is not altered, $I_0=0$, $I_j=\sum_{k=0}^{j-1}N_k$ for $j\in\mathbb{N}_{1:M-1}$ and $I_M=\sum_{k=0}^{M-1}N_k=N$. Following these definitions, the NLP, with shooting grid $\boldsymbol{G}_{0:M-1}$, can be written as:

$$\begin{aligned}\mathrm{NLP}_M:\quad &\min_{\boldsymbol{x}_{0:N},\boldsymbol{u}_{0:M-1}} \sum_{k=0}^{N-1} h(x_k,u_j,\hat{w}_j),\\ s.t.\quad & x_{k+1}=\phi(x_k,u_j,\hat{w}_j),\ k=\mathbb{N}_{0:N-1}\\ & (-z_{\max},-v_{\max})\le x_k\le(z_{\max},v_{\max}),\ k\in\mathbb{N}_{0:N},\\ & -u_{\max}\le u_j\le u_{\max},\ k\in\mathbb{N}_{0:M-1},\end{aligned}\tag{15}$$

where $u_j,\hat{w}_j$ is applied when $k\in\mathbb{N}_{I_j:I_{j+1}}$, $j\in\mathbb{N}_{0:M-1}$. Note that the state variable x is still discretised into N intervals to accurately capture its dynamic behaviour within the prediction horizon.

NLP_M covers the same prediction horizon timespan as NLP_N, using less control and wave prediction discretisation nodes, and hence has a smaller dimension. In general, a NLP can be solved using interior point (IP) methods or sequential quadratic programming (SQP). The former is suitable for solving a large-scale NLP, but is not trivial for activating warm-start, i.e. using optimal solutions from the previous sampling instant to initialise the current one. As a result, multiple distant local minima may be found from one sampling instant to another, leading to frequent switching between local minima and chattering in the control policy (Li, 2017). SQP methods, on the other hand, construct a sequence of quadratic program problems (QP) that can be solved by mature numerical solvers, with a possibility to use warm-start.

Using a SQP method to solve (15) gives rise to the following QP:

$$\begin{aligned}\min_{\Delta\mathbf{x}_{0:N},\Delta\mathbf{u}_{0:M}}\quad &\sum_{k=0}^{N-1}\left(\frac{1}{2}\begin{bmatrix}\Delta x_k\\ \Delta u_j\end{bmatrix}^T H_k\begin{bmatrix}\Delta x_k\\ \Delta u_j\end{bmatrix}+{g_k}^T\begin{bmatrix}\Delta x_k\\ \Delta u_j\end{bmatrix}\right)\\ &+\frac{1}{2}\Delta x_N^T H_N\Delta x_N^T+{g_N}^T\Delta x_N,\\ s.t.\quad &\Delta x_0=\hat{x}_0-x_0\\ &\Delta x_{k+1}=A_k\Delta x_k+B_k\Delta u_j+d_k,\\ &C_k\begin{bmatrix}\Delta x_k\\ \Delta u_j\end{bmatrix}+c_k\le 0,\quad \forall k=0,1,\dots,N-1,\\ &C_N\Delta x_N+c_N\le 0,\end{aligned}\tag{16}$$

where H_k is the approximated Hessian matrix, and $A_k=\frac{\partial\phi}{\partial x}(x_k,u_j,\hat{w}_j)$, $B_k=\frac{\partial\phi}{\partial u}(x_k,u_j,\hat{w}_j)$, $d_k=\phi(x_k,u_j,\hat{w}_j)-x_{k+1}$, $C_k=\frac{\partial r}{\partial(x,u)}(x_k,u_j,\hat{w}_j)$, $C_N=\frac{\partial l}{\partial x}(x_k,u_j,\hat{w}_j)$. Although an input MB technique has been used, problem (16) still contains many decision variables, and is mathematically a sparse problem. This hinders the use of warm-start strategies that are generally applicable to active-set methods, a class of optimisation methods which are implementable in real-time only for low-dimensional dense problems. This issue will be solved in Section 3.3 with the proposed *tailored condensing* strategy.

3.3. Tailored condensing to further accelerate calculation

The process of converting (16) to the following dense QP is termed *condensing*:

$$\begin{aligned}\min_{\Delta\boldsymbol{u}_{0:M-1}}\quad &\frac{1}{2}\Delta\boldsymbol{u}_{0:M-1}{}^{\top}H_c\Delta\boldsymbol{u}_{0:M-1}+g_c^{\top}\Delta\boldsymbol{u}_{0:M-1}\\ s.t.\quad &C_c\Delta\boldsymbol{u}_{0:M-1}+c_c\le 0,\end{aligned}\tag{17}$$

where matrices H_c,C_c and vectors g_c,c_c are obtained from (16) by exploiting the two equality constraint. Note that, for NMPC, the condensing step must be performed online at each sampling instant while, for linear MPC, it is an offline computation. The condensing step has a complexity of $\mathcal{O}(N^2)$ (Chen et al., 2020), which is costly in the case of WEC control, especially for small scale WEC prototypes.

To address this issue, a novel *tailored condensing* strategy is developed to suit the input MB approach introduced in Section 3.2, based on a recently developed condensing algorithm by the authors (Chen et al., 2020). As illustrated in Fig. 2, in the presence of wave prediction inaccuracies, a denser grid for shorter horizons and a coarser grid for longer horizons is adopted, leading to reduced computational complexity of the condensing step to $\mathcal{O}(N)$, by exploiting the unique structure of the input MB for WEC NMPC.

Design Procedures 1. *The proposed input-MB-based NMPC can be systematically designed by following these steps:*

Step 1: *Select a non-uniform grid $\boldsymbol{G}_{0:M-1}$ with decreasing density across the prediction horizon, as illustrated in Fig. 2(b);*
Step 2: *Perform multiple shooting, based on the non-uniform grid, assuming constant input and disturbance between each pair of neighbouring grid points, to obtain the sparse NLP_M (15);*
Step 3: *Implement the SQP method to obtain a series of sparse QP (16);*
Step 4: *Perform the tailored condensing step to obtain a dense QP (17);*
Step 5: *Solve the underlying dense QP using active-set methods.*

4. Estimation and prediction of the state and wave excitation force

So far, the development of the MB-based NMPC for WECs, in Section 3, assumes the availability of full state information $x(t)$ and the current and future wave excitation force $w(t)$. However, in operational conditions, the states associated with radiation force dynamics $x_r(t)$, and wave excitation force $w(t)$ are immeasurable and, thus, have to be estimated (Ringwood et al., 2023).

To facilitate the implementation of the proposed MB-based NMPC, estimation of the current $x(t)$ and $w(t)$ should first be addressed.

Assumption 1. The heave displacement $z(t)$ and heave velocity $v(t)$ of the float w.r.t. SWL is assumed to be directly measurable with sensors.[1]

The joint state and WEF estimation problem has been well-studied for WECs with linear dynamics. In Peña-Sanchez et al. (2019), a comprehensive benchmark study compares most of the existing WEF estimators, in terms of performance, computational complexity, and the risk of delays, in a computational fluid dynamics-based numerical wave tank. However, the estimation problem for a nonlinear WEC is more challenging.

To simplify the design process for the observer, the following input linear representation is introduced. An auxiliary unknown input is defined as:

$$\psi(t) := u(t) + w(t) - k_{nl}|v(t)|v(t), \tag{18}$$

where $u(t)$ is the known control input, $k_{nl}|v(t)|v(t)$ is the nonlinear viscosity force that can be calculated, and $w(t)$ is the unknown WEF to be estimated. The WEC model (7) can be rearranged into

$$\begin{aligned} \dot{x}(t) &= Ax(t) + B\psi(t), \\ y(t) &= Cx(t), \end{aligned} \tag{19}$$

where $y(t)$ denotes the measured output, with $C := [I_2, \ 0_{2\times n_r}]$.

Remark 1. Although the WEC dynamics are nonlinear, with an input linear representation as in (18)–(19), the same design procedures of linear WEF estimators, e.g., Kalman Filter with a Random Walk (KFRW) model, linear Unknown Input Observer (UIO), with the nonlinear core captured in $w(t) = \psi(t) + k_{nl}|v(t)|v(t) - u(t)$.

In this paper, a linear UIO design procedure can be followed, as detailed in Section II-G of Peña-Sanchez et al. (2019). Nonetheless, alternative linear WEF observation methods, such as KFRW, can also be employed with the linear input representation of (18)–(19).

With the designed WEF estimator, the current value of the complete state $x(t)$ and WEF $w(t)$ can be recovered, after a 'warming-up' period. Due to their simplicity, autoregressive (AR)-based wave predictors have been widely adopted in WEC control problems to generate noncausal information (see Pena-Sanchez et al., 2018b,a for comprehensive reviews on AR-based wave predictors). Next, the $w(t)$ predictor is briefly represented, using a standard AR formulation, for completeness.

With a sampling period of t_s, the p-step ahead predicted value of $w(t)$ can be expressed, using a discrete-time index k, i.e. $t = kt_s$, as follows:

$$\hat{w}_{k+p} = W_{k+p}^{-H}\Psi, \tag{20}$$

where $W_{k+p}^{-H} := [\hat{w}_{k+p-1} \ \ \hat{w}_{k+p-2} \ \ \dots \ \ \hat{w}_{k+p-H}]$, H is the order of the model, and $\Psi \in \mathbb{R}^H$ are the AR coefficients to be identified. In (20), $\hat{w}_{k+i}$ takes the estimated value of $w((k+i)t_s)$ from the WEF estimator, when $i < 0$, but is calculated recursively using an AR predictor (20), when $i \geq 0$.

Given a set of training data of dimension N_{tr} (corresponding to length $T_{tr} = N_{tr}t_s$), the AR coefficients Ψ can be identified by minimising the following one-step cost:

$$J_{AR} = \sum_{k=H+1}^{N_{tr}} (w_k - W_k^{-H}\Psi)^2, \tag{21}$$

using batch, or recursive, least squares.

By recursively using (20), an N-step-ahead wave excitation force prediction can be obtained at each time instant k which, after interpolation, can be expressed using a continuous time index t as $\hat{w}(t+p)$, for $0 < p \leq T$ with $T := Nt_s$.

[1] Motion can be typically measured using an inertial measurement unit (IMU).

Table 1
Simulated device specifications.

Description	Notation	values
Stiffness	k_s	3866 N/m
Float mass	m_s	242 kg
Added mass	m_a	83.5 kg
Total mass	m	325.5 kg
Nonlinear damping coefficient	k_{nl}	48 kg/m
Input force limit	$u_{\max}$	3 kN
Heave displacement limit	$z_{\max}$	2 m
Heave velocity limit	$v_{\max}$	10 m/s
Energy loss coefficient	r	0.1 m/(kN s)

Table 2
The parameters of the sea states used to generate the wave excitation force datasets for controller simulation and AR predictor training.

	H_s(m)	T_p(s)	γ
Sea State I (test data set 1)	2	3	4
Sea State II (test data set 2)	4	3.5	4
Sea State III (AR training data set)	3	2	4

5. Numerical simulation

This section provides simulation results using known wave profiles to verify the efficacy of the proposed method. The parameters used here reflect the hydrodynamics of a small-scale PA-WEC, as specified in Table 1.

The state-space model for radiation force dynamics (6) has the following parameters

$$A_r = \begin{bmatrix} 0 & 0 & -17.9 \\ 1 & 0 & -17.7 \\ 0 & 1 & -4.41 \end{bmatrix}, \quad B_r = \begin{bmatrix} 38.6 \\ 379 \\ 89 \end{bmatrix}, \quad C_r = \begin{bmatrix} 0 \\ 0 \\ 1 \end{bmatrix}^{\top}.$$

Since the model and the cost function are both nonlinear, the terminal cost function h_N in (12), or h_M in (15), is not considered. The MB-NMPC is designed following Design Procedure 1.

To estimate the WEF, with the input linear representation of (18)–(19), an UIO-based WEF estimator is designed using (25)–(26) from Peña-Sanchez et al. (2019).

The simulations use two WEF profiles, both generated from JONSWAP spectra (Hasselmann et al., 1973), with the same peakedness factor γ, but with different significant wave heights H_s, and peak periods T_p, shown in Table 2, which are chosen considering the scaling due to the use of a small-scale WEC, to simulate a low sea state and a high sea state, respectively. The WEF dynamic model used to generate the WEF profile is described by:

$$\begin{cases} \dot{x}_e(t) = A_e x_e(t) + B_e \eta(t) \\ w(t) = C_e x_e(t) \end{cases} \tag{22}$$

where the WEF dynamic coefficients A_e, B_e, C_e are the same as those specified in Eqs. (47)–(49 of Yu and Falnes (1995); x_e represents the state of the WEF dynamics (22); $\eta(t)$ denotes the sea elevation derived from the JONSWAP spectrum.

To predict the WEF, a 50th-order AR predictor is designed according to (20) and parameterised using data collected from Sea State III (detailed in Table 2). Here, to verify the robustness of the proposed MB-NMPC against prediction errors, a different sea state is deliberately chosen to train the AR model, to simulate the potential mismatch of an AR predictor due to the changing meteorological conditions.

A snapshot of a 3-s wave excitation force and the predicted value using the AR predictor, is shown in Fig. 3. Here, to test the robustness of the proposed MB-NMPC, the AR predictor is deliberately designed with a very short lookback horizon (0.5 s) to generate a wave prediction with rapidly decreasing accuracy.

As the existing MPC design principles vary case by case, in this section, we benchmark the MB-NMPC against the following three representative MPC settings:

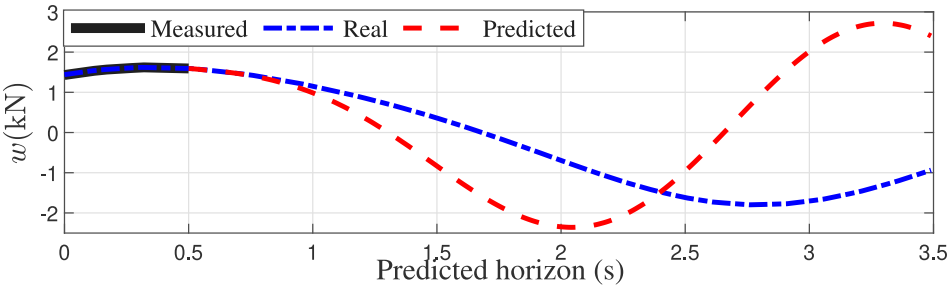

Fig. 3. An 3-s wave excitation force profile segment. The 50th-order AR predictor uses the first 0.5 s of measured data in Test data set 1 to predict 3 s of wave excitation force ahead.

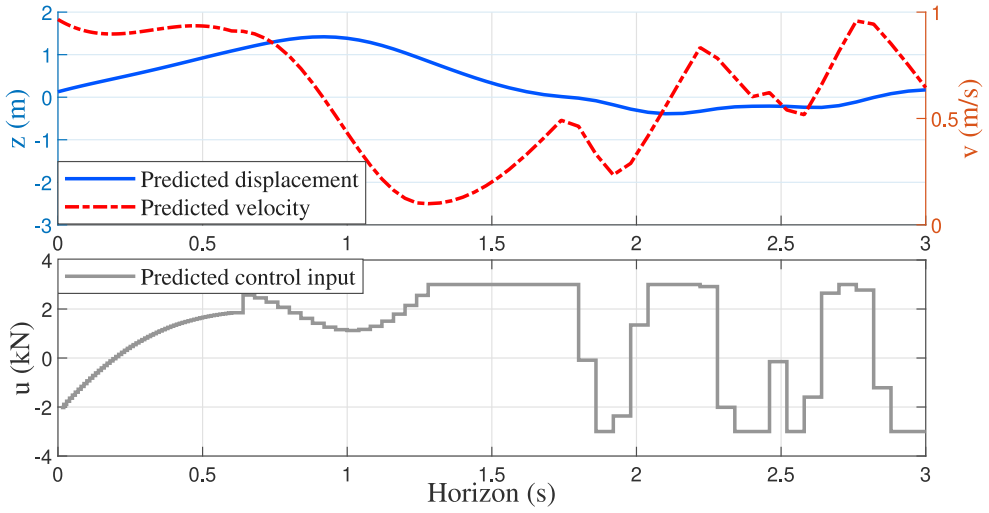

Fig. 4. A snapshot of predicted state and input trajectories, using MB-NMPC, with a 3-s control horizon.

1. A standard NMPC with a uniform grid, using the NLP_N (12) formulation, referred to as 'S-NMPC', representing existing works on NMPC such as Guerrero-Fernandez et al. (2023) and Huang et al. (2024),
2. A linear MPC (LMPC), formed by omitting the nonlinear term $f_{nl}(t)$ from (4), referred to as 'LMPC-1', representing existing LMPC formulations such as Bracco et al. (2020), Zhan et al. (2020), and
3. A LMPC, formed by using an equivalent linear damping term to approximate the nonlinear term, i.e., $f_{nl}(t) \approx -41\,\text{kg/s} \times v(t)$ in (4), referred to as 'LMPC-2', representing existing LMPC formulations such as Bonfanti et al. (2024).

The sampling frequency, for all controllers, is set to 100 Hz. The S-NMPC and both LMPCs utilise a uniform $\Delta t = 0.01$ s as the length of each shooting interval, equivalent to a prediction length of $T = \Delta t \times N$. In contrast, the MB-NMPC is configured to partition the prediction horizon into three sub-windows. The first sub-window consists of $N/5$ blocks, each of which has a uniform $\Delta t_1 = \Delta t = 0.01$ s; the second and third sub-windows have $2N/25$ blocks, with uniform $\Delta t_2 = 4\Delta t = 0.04$ s, and the block in the third sub-window has a uniform $\Delta t_3 = 6\Delta t = 0.06$ s. Fig. 4 shows a snapshot of the predicted state and input trajectories for the MB-NMPC. Note that the input partition for the MB-NMPC is in line with the prediction accuracy of the WEF, as shown in Fig. 3.

The simulation is performed using MATLAB R2021a, running under Windows 11, using the real-time NMPC toolbox MATMPC (Chen et al., 2019) as the online solver, on a PC with Intel Core i7-11700KF, running at 3.60 GHz. The NLP problems stemming from both S-NMPC and MB-NMPC are solved using the same Real-time Iteration (RTI) method (Diehl et al., 2002), in which a single QP problem is firstly condensed (Algorithms 1 and 2 of Chen et al. (2020) for MB-NMPC, and Algorithm 1 of Frison et al. (2016) for S-NMPC, respectively), and then solved using existing library QPOASES (Ferreau et al., 2014), with warm-start activated.

In Fig. 5, the force, position, and velocity trajectories of the WEC over the 50-s time simulation are given, *assuming the WEF is perfectly known*. In this ideal scenario, S-NMPC produces 43.36 kJ of energy over 50 s, which can be viewed as a reference basis representing the maximum achievable performance in those simulation settings. The performance of MB-NMPC, with the input MB modification, recovers 99.31% of performance, while the two LMPCs can only achieve 75.86% and 89.21% of the energy output, respectively. Next, to test the robustness of four MPC algorithms in the presence of WEF prediction errors, in Fig. 6, the same simulation is repeated, but assuming the WEF is *predicted imperfectly*, using the AR predictor trained for a different sea state. Fig. 3 shows a snapshot of the WEF predicted by the AR model, where the discrepancy substantially increases beyond a 1-s horizon.

By comparing Fig. 6 with Fig. 5, it can be seen that all four MPC algorithms suffer from performance degradation. However, MB-NMPC can produce 41.30 kJ of energy, recovering 95.25% of the ideal performance, while, S-NMPC produces just 39.81 kJ of energy, representing a more significant performance degradation of 91.81% from the ideal case. This shows the efficacy of the proposed input MB strategy that explicitly considers the decreasing WEF prediction accuracy along the horizon, proving the 'less is more' concept. In this case, the two LMPC designs produce significantly less energy, with 26.13 kJ for LMPC-1 and 32.92 kJ for LMPC-2.

Next, we conduct 20 scenarios of the simulation based on 20 segments of the WEF profile, generated using the JONSWAP spectrum with the same peakedness factor, $\gamma = 4$, but with a deliberately introduced randomised shift of up to 5% on $H_s = 2$ m and $T_p = 3$ s, to test the reliability of the algorithm. Four MPC algorithms, and

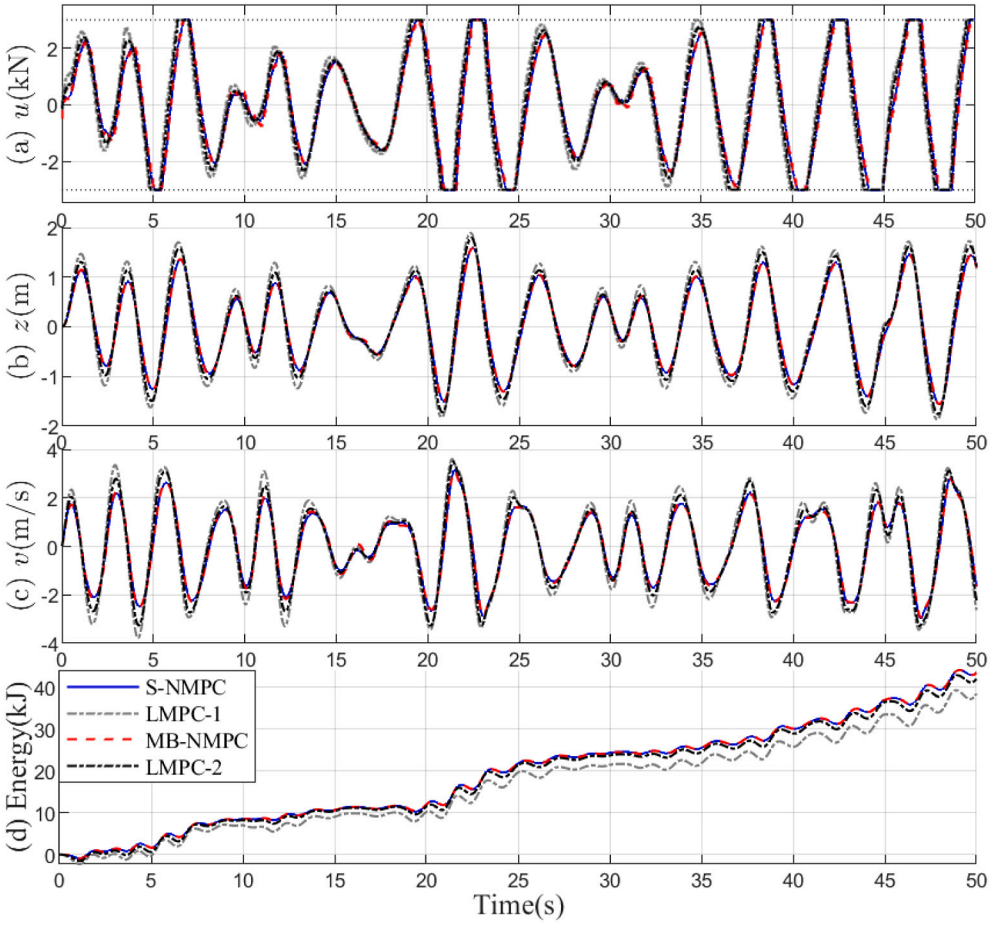

Fig. 5. A 50-s comparative time simulation showing (i) S-NMPC (blue solid line); (ii) LMPC-1 (grey dashed and dotted line); (iii) MB-NMPC (red dashed line); LMPC-2 (black dashed line), using Test data set 1: (a) control input ; (b) heave displacement; (c) heave velocity; (d) converted energy. The prediction horizon is $T = 1.5$ s. For a uniform NMPC and LMPC grid, the number of shooting intervals is $N = 100$; For MB-NMPC, the number of blocks is $M = 36$. The wave excitation force is assumed to be perfectly known, i.e. the AR predictor is not used for this case, focusing exclusively on control performance.

the AR WEF predictors, adopt the same settings as in the previous simulation. Fig. 7(a)–(b) illustrates the percentage of performance loss, relative to the idealised NMPC case, and the average computation time required to complete one online optimisation at each sampling instant, respectively. It can be observed that MB-NMPC demonstrates the best consistency among the four MPC algorithms, particularly in terms of computation speed, which exhibits minimal variation. Furthermore, there are no exceptional cases of instability or constraint violations. This consistency property of MB-NMPC is crucial for real-time control testing and implementation.

To further demonstrate the efficacy of the MB-NMPC, in dealing with WEF prediction error, and in reducing computational load, in Figs. 8–10, two sets of comparative simulations are presented, based on Sea States 1–2, which result in different levels of constraint saturation. Controllers and AR predictors adopt the same setting of in Figs. 5–6.

It can be seen, from Figs. 8–9 that when imperfect WEF prediction is provided by the AR predictor, the MB-NMPC outperforms the SMPC, taking into account less inaccurate wave excitation force prediction, and hence suffering less control performance degradation. Figs. 8–9 also show that, the LMPC has inferior performance, with almost all prediction horizon settings, both with/without the AR predictor. An intriguing observation is that, the energy produced by both NMPC schemes gradually decreases as the prediction horizon increases, due to the growing prediction errors in NMPC problems with longer horizons. For a prediction horizon of less than 1 s, the performance of all controllers suffers, since the prediction horizon is inadequate to accurately solve the noncausal control problem.

The computation time at each sampling instant, for each controller call, of S-NMPC, MB-NMPC and LMPC, is collected and presented in Fig. 10. It can be seen that, when the prediction horizon increases from $T = 0.5$ s to $T = 2$ s, the MB-NMPC has a much shorter computational time than SNMPC, in terms of median and maximum values. Over a prediction horizon range of 0.5–2 s, the median runtime ratio (S-NMPC/MB-NMPC) is maintained >2, which means MB-NMPC is more than twice as fast as S-NMPC. The reason is two-fold: (1) MB-NMPC has much fewer decision variables due to input MB, hence, the dimension of its optimisation problem is smaller; (2) the tailored condensing strategy further reduces the computational cost. On the other hand, LMPC is the fastest among the three algorithms, since it does not need to compute Hessian and Jacobian matrices online. However, as the prediction horizon grows, the computation time of LMPC varies much more heavily than MB-NMPC. This is because LMPC encounters many more input saturation instants, as shown in Figs. 5 and 6, which leads to more active constraints and QP iterations. This phenomenon is validated by comparing the two sub-figures in Fig. 10, where the computation time variation of LMPC for the Sea State 1 is smaller than that for Sea State 2 (with higher wave height).

It is worth noting that the MB-NMPC scheme used in this simulation can be tuned with more moving blocks to increase prediction accuracy at the cost of more computational time, or with fewer moving blocks to decrease prediction accuracy for less computation. This tuning process provides flexibility of the input MB NMPC scheme, but is non-trivial and affects the recursive feasibility and stability of the resulting NMPC scheme. For more details on this topic, please refer to Chen et al. (2020).

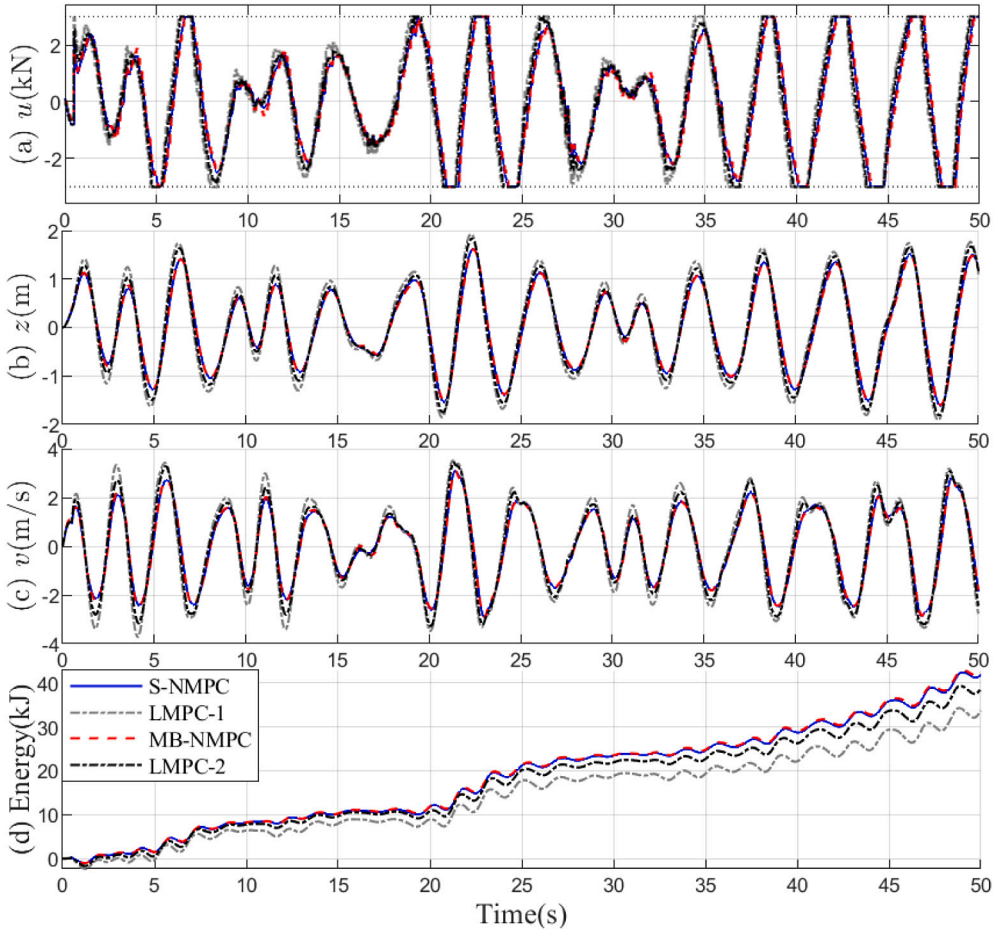

Fig. 6. A 50-s comparative time simulation among (i) S-NMPC (blue solid line); (ii) LMPC-1 (grey dashed and dotted line); (iii) MB-NMPC (red dotted line), LMPC-2 (black dashed line), using Test data set 1: (a) control input; (b) heave displacement; (c) heave velocity; (d) converted energy. The prediction horizon is $T = 1.5$ s. For S-NMPC and LMPC, the number of shooting intervals is $N = 100$; for MB-NMPC, the number of blocks is $M = 36$. The wave excitation force is predicted within each prediction horizon using a 50th-order AR predictor.

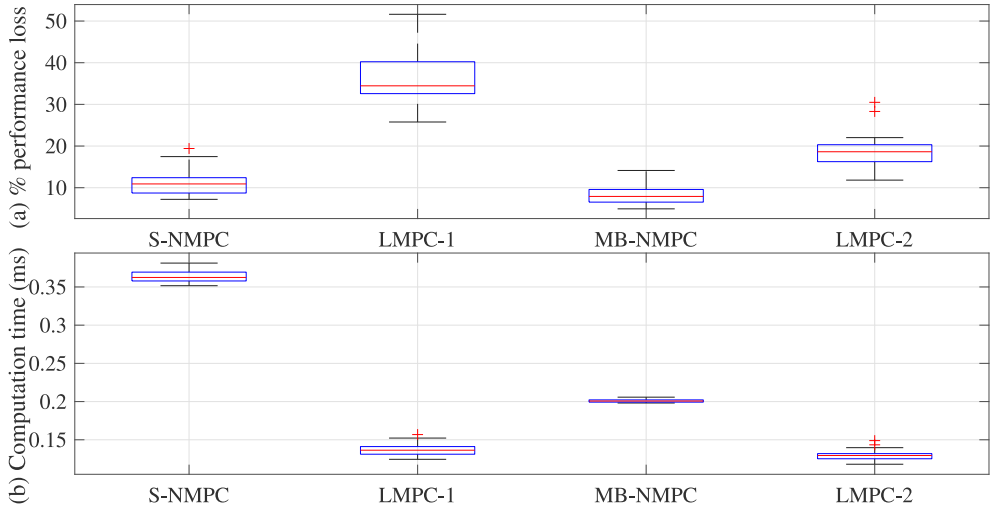

Fig. 7. Control reliability test: (a) percentage of performance loss with respect to the NMPC using conceptual unrealistic 100% accurate WEF prediction; (b) the average computational time of completing one optimisation at each sampling instant. The controllers and AR WEF predictor adopt the same settings as in Figs. 5–6.

Finally, we test the performance of the proposed MB-NMPC using a segment of a 50-s WEF profile, shown in Fig. 11(a), generated using the same excitation dynamics (22) and sea wave elevation data collected off the English Atlantic coast. The AR predictor is retrained, based on a JONSWAP spectrum, with a significant wave height of 3 m, a peak period of 6 s and the same peakedness factor of 4. All NMPCs adopt the same prediction horizon of 1.5 s. Fig. 11(b) and (c) illustrate the response of the control input u and the accumulated energy, respectively. The energy generated in the 50-s simulation using MB-NMPC reaches 24.88 kJ, outperforming the S-NMPC without using the non-uniform

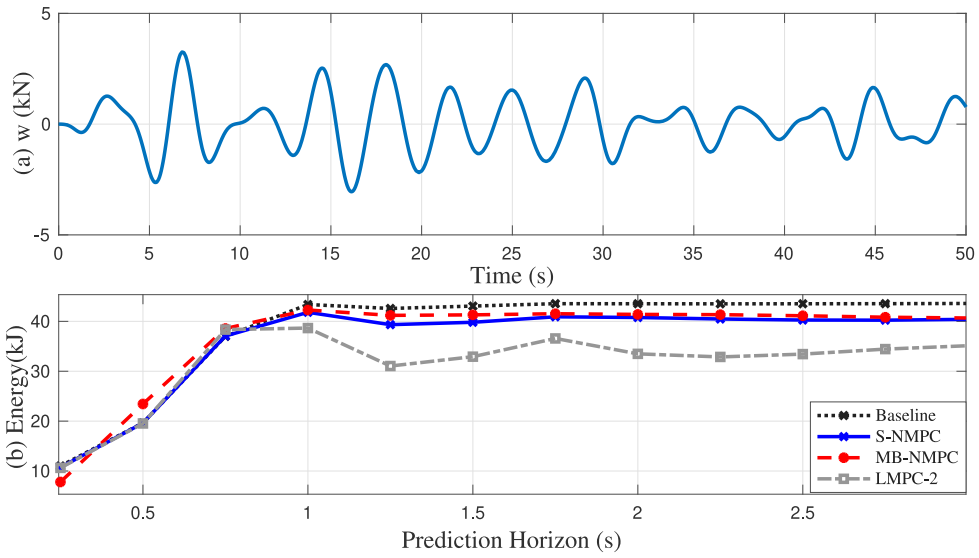

Fig. 8. Comparative time simulation with Test Dataset 1 among the three MPC schemes (Blue: S-NMPC; Red: MB-NMPC; Grey: LMPC-2) using reparametrised AR predictor, compared against a "Baseline" representing the ideal performance of NMPC with 100% accurate WEF prediction: (a) the 50-s WEF profile; (b) energy generated.

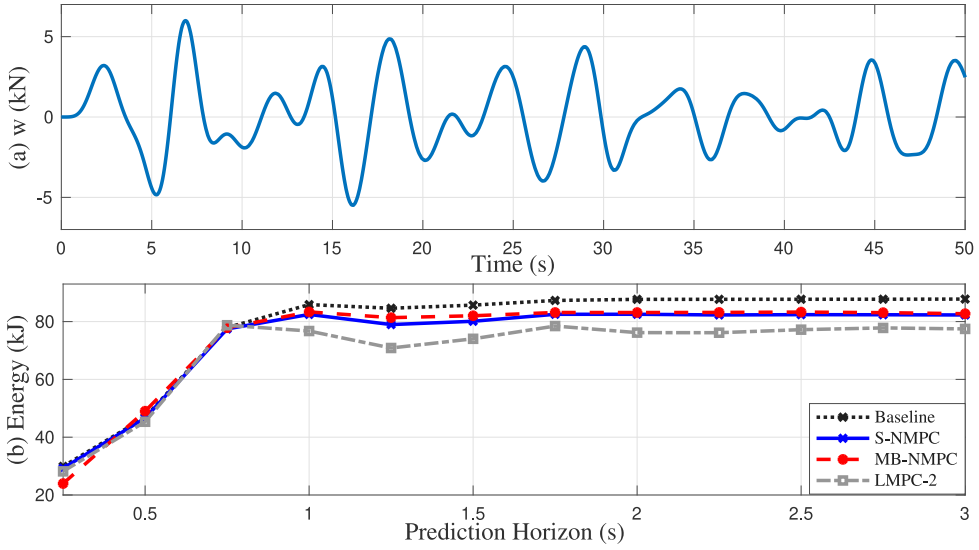

Fig. 9. Comparative time simulation with Test Dataset 2 among the same controllers and AR predictor as in Fig. 8: (a) the 50-s WEF profile; (b) energy generated.

grid by 1.93%, and recovers 93.15% performance of the baseline NMPC using 100% accurate wave prediction.

This result further demonstrates the advantages of MB-NMPC across various simulation settings.

6. Conclusion

This paper develops a novel computationally-efficient nonlinear model predictive control (NMPC) scheme for the wave energy converter (WEC) energy maximisation control problem, using an input move blocking (MB) technique. Considering the decreased wave prediction accuracy, as the prediction horizon increases, MB-NMPC defines a non-uniform shooting interval, emphasising shorter horizons with a higher confidence level, and providing a relatively sparse solution for longer horizons. The non-definite cost function of the WEC NMPC problem introduces challenges to the convergence and continuity of the solution. To resolve those problems, and to further reduce the computational load, a tailored condensing strategy is developed using a modified active-set method, allowing a 'warm start', i.e., using the previous optimal solution as the starting search points. Numerical examples validate that, compared with existing NMPC formulation without using input MB, the novel MB-NMPC scheme achieves smoother input trajectories and a better energy conversion, with an additional significant reduction in computation. MATLAB implementation results show that real-time sampling rates are easily achievable. These results open the door for real-time implementation of NMPC for WECs with nonlinear hydrodynamics, to realise their full energy conversion potential. We acknowledge that the accuracy of the wave predictor can vary across different sea states, while the input-MB NMPC developed in this paper employs a fixed meshing policy. Our future work will focus on developing adaptive MB strategies to better accommodate the varying wave excitation force prediction accuracies in different sea states.

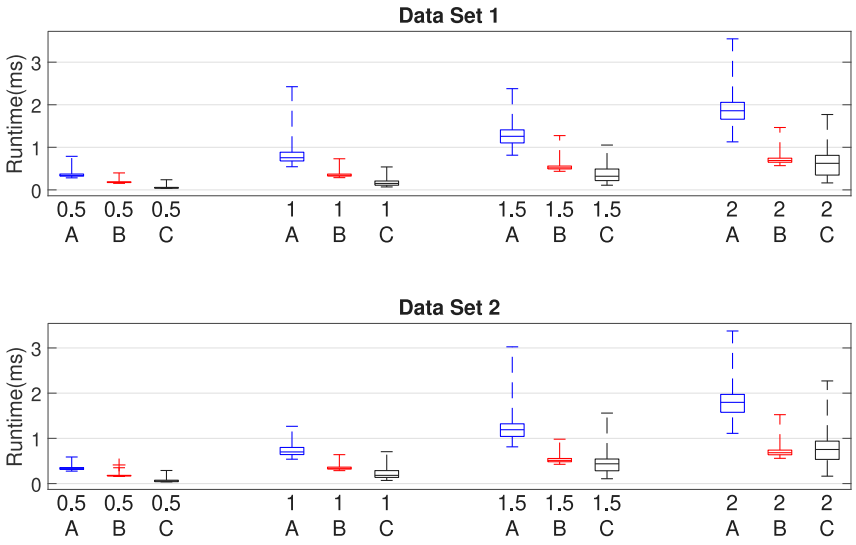

Fig. 10. Median/range runtimes for each sampling instant of S-NMPC (A), MB-NMPC (B) and LMPC-2 (C) using different prediction horizons ($T = 0.5, 1, 1.5, 2$ s).

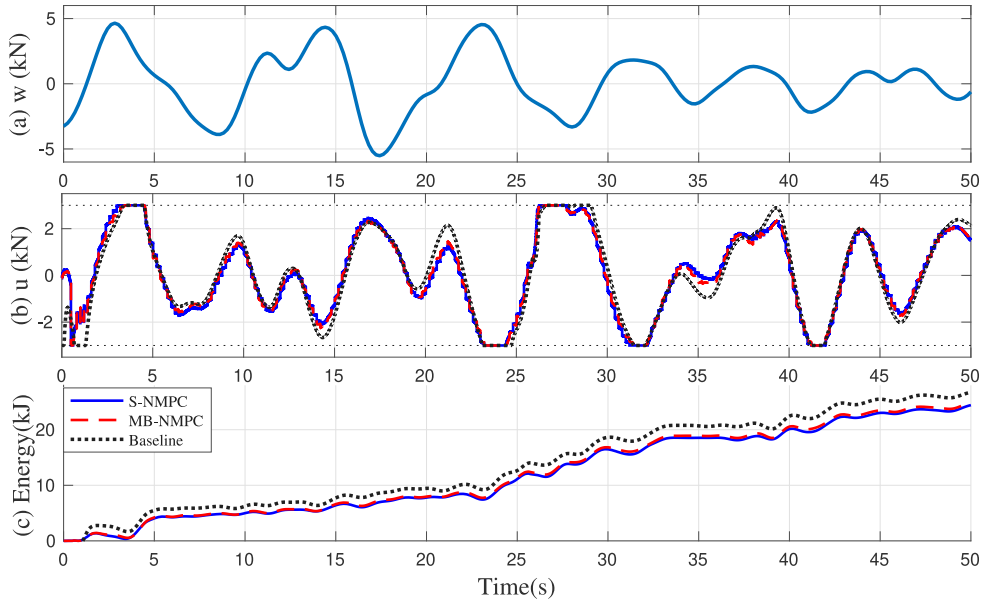

Fig. 11. Time simulation using (i) S-NMPC, and (ii) MB-NMPC, compared against a "Baseline" representing the ideal performance of NMPC with 100% accurate WEF prediction. (a) the 50-s WEF profile generated using the excitation dynamics (22) and a 50-s segment of real sea wave elevation data; (b) control input; (c) energy generated.

CRediT authorship contribution statement

Siyuan Zhan: Writing – original draft, Investigation, Conceptualization. **Yutao Chen:** Writing – review & editing, Software, Methodology, Funding acquisition. **John V. Ringwood:** Supervision.

Funding

This work was supported by the National Natural Science Foundation of China [grant number 62403134], the Natural Science Foundation of Fujian Province [grant number 2022J05025], the Fujian Provincial Department of Education Young Teachers' Education Research Project [grant number JAT210032] and the Fuzhou University Research Initiation Project [grant number XRC21075]. John Ringwood is grateful for the support of Taighde Éireann (Research Ireland) in respect of the Research Centre for Energy, Climate and Marine, Ireland [grant number 12/RC/2302 P2].

Declaration of competing interest

The authors declare that they have no known competing financial interests or personal relationships that could have appeared to influence the work reported in this paper.

Acknowledgement

The authors would like to thank Mrs. CarrieAnne Barry, for her help in proofreading the paper.

References

Babarit, A., Clément, A.H., 2006. Optimal latching control of a wave energy device in regular and irregular waves. Appl. Ocean Res. 28 (2), 77–91.

Bacelli, G., Genest, R., Ringwood, J.V., 2015. Nonlinear control of flap-type wave energy converter with a non-ideal power take-off system. Annu. Rev. Control 40, 116–126.

Belmont, M., Christmas, J., Dannenberg, J., Hilmer, T., Duncan, J., Duncan, J., Ferrier, B., 2014. An examination of the feasibility of linear deterministic sea wave prediction in multidirectional seas using wave profiling radar: Theory, simulation, and sea trials. J. Atmos. Ocean. Technol. 31 (7), 1601–1614.

Bock, H.G., Plitt, K.-J., 1984. A multiple shooting algorithm for direct solution of optimal control problems. IFAC Proc. Vol. 17 (2), 1603–1608.

Bonfanti, M., Faedo, N., Mattiazzo, G., 2024. Towards efficient control synthesis for nonlinear wave energy conversion systems: impedance-matching meets the spectral-domain. Nonlinear Dynam. 1–25.

Bracco, G., Canale, M., Cerone, V., 2020. Optimizing energy production of an inertial sea wave energy converter via model predictive control. Control Eng. Pract. 96, 104299.

Chen, Y., Bruschetta, M., Picotti, E., Beghi, A., 2019. Matmpc-a matlab based toolbox for real-time nonlinear model predictive control. In: 2019 18th European Control Conference. ECC, Naples, Italy, pp. 3365–3370.

Chen, Y., Scarabottolo, N., Bruschetta, M., Beghi, A., 2020. Efficient move blocking strategy for multiple shooting-based non-linear model predictive control. IET Control Theory Appl. 14 (2), 343–351.

Cummins, W., 1962. The impulse response function and ship motions. Schiffstechnik 101–109.

Demonte Gonzalez, T., Anderlini, E., Yassin, H., Parker, G., 2024. Nonlinear model predictive control of heaving wave energy converter with nonlinear Froude–Krylov forces. Energies 17 (20), 5112.

Diehl, M., Bock, H.G., Schlöder, J.P., Findeisen, R., Nagy, Z., Allgöwer, F., 2002. Real-time optimization and nonlinear model predictive control of processes governed by differential-algebraic equations. J. Process Control 12 (4), 577–585.

Faedo, N., Giorgi, G., Ringwood, J., Mattiazzo, G., 2022a. Optimal control of wave energy systems considering nonlinear Froude–Krylov effects: control-oriented modelling and moment-based control. Nonlinear Dynam. 109 (3), 1777–1804.

Faedo, N., Giorgi, G., Ringwood, J.V., Mattiazzo, G., 2022b. Nonlinear moment-based optimal control of wave energy converters with non-ideal power take-off systems. In: 41st ASME Intl. Conf. on Offshore Mechanics and Arctic Eng.. OMAE, Hamburg, Germany, pp. 1–10.

Faedo, N., Mattiazzo, G., Ringwood, J.V., 2022c. Robust energy-maximising control of wave energy systems under input uncertainty. In: 2022 Euro. Control Conf.. ECC, London, UK, pp. 614–619.

Faedo, N., Olaya, S., Ringwood, J.V., 2017. Optimal control, MPC and MPC-like algorithms for wave energy systems: An overview. IFAC J. Syst. Control 1, 37–56.

Faedo, N., Scarciotti, G., Astolfi, A., Ringwood, J.V., 2021. Nonlinear energy-maximizing optimal control of wave energy systems: A moment-based approach. IEEE Trans. Control Syst. Technol. 29 (6), 2533–2547.

Falnes, J., 2002. Ocean Waves and Oscillating Systems: Linear Interactions Including Wave-Energy Extraction. Cambridge University Press.

Ferreau, H.J., Kirches, C., Potschka, A., Bock, H.G., Diehl, M., 2014. qpOASES: A parametric active-set algorithm for quadratic programming. Math. Program. Comput. 6 (4), 327–363.

Frison, G., Kouzoupis, D., Jø rgensen, J.B., Diehl, M., 2016. An efficient implementation of partial condensing for nonlinear model predictive control. In: IEEE 55th Conference on Decision and Control (CDC), Las Vegas, USA. pp. 4457–4462.

Fusco, F., Ringwood, J.V., 2010. Short-term wave forecasting for real-time control of wave energy converters. IEEE Trans. Sustain. Energy 1 (2), 99–106.

Genest, R., Ringwood, J.V., 2016. Receding horizon pseudospectral control for energy maximization with application to wave energy devices. IEEE Trans. Control Syst. Technol. 25 (1), 29–38.

Giorgi, G., Ringwood, J., 2017. Consistency of viscous drag identification tests for wave energy applications. In: Proceedings of EWTEC, Cork, Ireland.

Guerrero-Fernandez, J.L., González-Villarreal, O.J., Rossiter, J.A., 2023. Efficiency-aware nonlinear model-predictive control with real-time iteration scheme for wave energy converters. Internat. J. Control 96 (8), 1909–1921.

Guerrero-Fernández, J., González-Villarreal, O.J., Rossiter, J.A., Jones, B., 2020. Model predictive control for wave energy converters: A moving window blocking approach. IFAC-PapersOnLine 53 (2), 12815–12821.

Guerrero-Fernández, J.L., Tom, N.M., Rossiter, J.A., 2022. Nonlinear model predictive control based on real-time iteration scheme for wave energy converters using WEC-sim. In: International Conference on Offshore Mechanics and Arctic Engineering. vol. 85932, American Society of Mechanical Engineers, V008T09A076.

Guo, B., Ringwood, J.V., 2021. A review of wave energy technology from a research and commercial perspective. IET Renew. Power Gener. 15 (14), 3065–3090.

Haider, A.S., Brekken, T.K., McCall, A., 2021. Application of real-time nonlinear model predictive control for wave energy conversion. IET Renew. Power Gener. 15 (14), 3331–3340.

Hasselmann, K., Barnett, T., Bouws, E., Carlson, H., Cartwright, D., Enke, K., Ewing, J., Gienapp, H., Hasselmann, D., Kruseman, P., et al., 1973. Measurements of wind-wave growth and swell decay during the joint north sea wave project (JONSWAP). Ergänzungsheft 8-12.

Houska, B., Ferreau, H.J., Diehl, M., 2011. ACADO toolkit—An open-source framework for automatic control and dynamic optimization. Opt. Control Appl. Methods 32 (3), 298–312.

Huang, X., Lin, Z., Chen, K., Zhou, J., Xiao, X., 2024. Improving wave-to-wire efficiency of direct-drive wave energy converters with loss-aware model predictive control and variable DC voltage control. IEEE Trans. Ind. Electron..

Kody, A., Tom, N., Scruggs, J., 2019. Model predictive control of a wave energy converter using duality techniques. In: 2019 American Control Conference. ACC, Philedelphi, USA, pp. 5444–5451.

Li, G., 2017. Nonlinear model predictive control of a wave energy converter based on differential flatness parameterisation. Internat. J. Control 90 (1), 68–77.

Li, G., Weiss, G., Mueller, M., Townley, S., Belmont, M.R., 2012. Wave energy converter control by wave prediction and dynamic programming. Renew. Energy 48, 392–403.

Mérigaud, A., Ringwood, J.V., 2017. Improving the computational performance of nonlinear pseudospectral control of wave energy converters. IEEE Trans. Sustain. Energy 9 (3), 1419–1426.

Paparella, F., Monk, K., Winands, V., Lopes, M., Conley, D., Ringwood, J.V., 2014. Up-wave and autoregressive methods for short-term wave forecasting for an oscillating water column. IEEE Trans. Sustain. Energy 6 (1), 171–178.

Pena-Sanchez, Y., Garcia-Abril, M., Paparella, F., Ringwood, J.V., 2018a. Estimation and forecasting of excitation force for arrays of wave energy devices. IEEE Trans. Sustain. Energy 9 (4), 1672–1680.

Pena-Sanchez, Y., Mérigaud, A., Ringwood, J.V., 2018b. Short-term forecasting of sea surface elevation for wave energy applications: The autoregressive model revisited. IEEE J. Ocean. Eng. 45 (2), 462–471.

Peña-Sanchez, Y., Windt, C., Davidson, J., Ringwood, J.V., 2019. A critical comparison of excitation force estimators for wave-energy devices. IEEE Trans. Control Syst. Technol. 28 (6), 2263–2275.

Penalba, M., Giorgi, G., Ringwood, J.V., 2017a. Mathematical modelling of wave energy converters: a review of nonlinear approaches. Renew. Sustain. Energy Rev. 78, 1188–1207.

Penalba, M., Kelly, T., Ringwood, J., 2017b. Using NEMOH for modelling wave energy converters: A comparative study with WAMIT. In: Proceedings of EWTEC, Cork, Ireland.

Richter, M., Magana, M.E., Sawodny, O., Brekken, T.K., 2012. Nonlinear model predictive control of a point absorber wave energy converter. IEEE Trans. Sustain. Energy 4 (1), 118–126.

Ringwood, J.V., Zhan, S., Faedo, N., 2023. Empowering wave energy with control technology: Possibilities and pitfalls. Annu. Rev. Control 55, 18–44.

Tom, N., Yeung, R.W., 2014. Nonlinear model predictive control applied to a generic ocean-wave energy extractor. J. Offshore Mech. Arct. Eng. 136 (4).

Unneland, K., 2007. Identification and order reduction of radiation force models of marine structures, *Fakultet for informasjonsteknologi, matematikk og elektroteknikk*.

Windt, C., Faedo, N., Penalba, M., Dias, F., Ringwood, J.V., 2021. Reactive control of wave energy devices–the modelling paradox. Appl. Ocean Res. 109, 102574.

Yu, Z., Falnes, J., 1995. State-space modelling of a vertical cylinder in heave. Appl. Ocean Res. 17 (5), 265–275.

Zhan, S., Li, G., 2019. Linear optimal noncausal control of wave energy converters. IEEE Trans. Control Syst. Technol. 27 (4), 1526–1536.

Zhan, S., Na, J., Li, G., Wang, B., 2020. Adaptive model predictive control of wave energy converters. IEEE Trans. Sustain. Energy 11 (1), 229–238.

Zou, S., Abdelkhalik, O., Robinett, R., Bacelli, G., Wilson, D., 2017. Optimal control of wave energy converters. Renew. Energy 103, 217–225.